MedBLIP: Bootstrapping Language-Image Pre-training from 3D Medical Images and Texts

Qiuhui Chen, Xinyue Hu, Zirui Wang, Yi Hong[*]
Shanghai Jiao Tong University

Abstract

Vision-language pre-training (VLP) models have been demonstrated to be effective in many computer vision applications. In this paper, we consider developing a VLP model in the medical domain for making computer-aided diagnoses (CAD) based on image scans and text descriptions in electronic health records, as done in practice. To achieve our goal, we present a lightweight CAD system MedBLIP, a new paradigm for bootstrapping VLP from off-the-shelf frozen pre-trained image encoders and frozen large language models. We design a MedQFormer module to bridge the gap between 3D medical images and 2D pre-trained image encoders and language models as well. To evaluate the effectiveness of our MedBLIP, we collect more than 30,000 image volumes from five public Alzheimer's disease (AD) datasets, i.e., ADNI, NACC, OASIS, AIBL, and MIRIAD. On this largest AD dataset we know, our model achieves the SOTA performance on the zero-shot classification of healthy, mild cognitive impairment (MCI), and AD subjects, and shows its capability of making medical visual question answering (VQA). The code and pre-trained models is available online: https://github.com/Qybc/MedBLIP.

1 Introduction

Electronic health records (EHR), e.g., radiology images, lab and test results, and patient demographics, are often used in clinical diagnosis. For instance, to diagnose Alzheimer's Disease (AD), apart from brain imaging, physicians also use physical and neurological exams and diagnostic tests, with these test results presented in the text form. In past decades, researchers have gradually collected a large number of EHRs, e.g., ADNI Petersen et al. [2010], NACC Beekly et al. [2007], OASIS Marcus et al. [2007], for studying AD. However, learning how to make diagnoses based on these EHRs, especially how to fuse these medical data from different resources and in different forms, e.g., images and texts, is still a challenging task in computer-aided diagnosis (CAD).

Recently, large vision language pre-training (VLP) models, e.g., CLIP Radford et al. [2021], BLIP Li et al. [2022], BLIP-2 Li et al. [2023], have achieved great success in many downstream computer vision applications, such as classification Bao et al. [2022], segmentation Xu et al. [2021]. These VLP models learn multi-modal representations from large image and text datasets, by aligning their features into a common space for learning. In the medical domain, researchers propose Medical Bootstrapping Language-Image Pre-training (MedCLIP) Wang et al. [2022], which learns generic representation from large-scale medical image-text pairs. This pre-trained medical model presents its generalization to various medical tasks, especially where limited medical data or labels are available for learning. However, most existing VLP models handle the situation that texts are corresponding textual descriptions of their paired images, such as image captions or medical reports.

In this paper, we consider another scenario where images and texts provide complementary information, that is, texts include additional information except for medical scans in EHRs, e.g., the

---

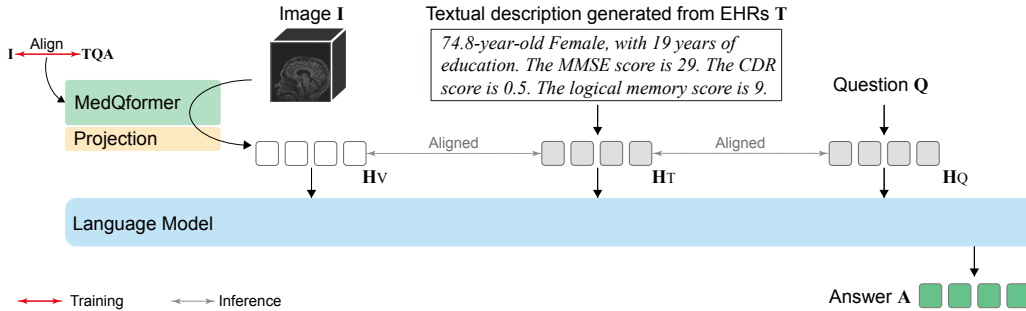[*]Corresponding Author: yi.hong@sjtu.edu.cn

Figure 1: Architecture overview of our proposed MedBLIP, a CAD system designed for medical diagnosis with electronic health records via multimodel representation learning in a language model.

age, gender, and lab results of a subject, to make an informed CAD decision. Our goal is to learn a VLM that suits this CAD scenario, which has multi-model intelligence to fuse different types of medical data, e.g., 3D medical scans and texts that contain complementary information from EHRs for CAD. Here, we need to address three problems: (1) How to extend a 2D image encoder to extract features from 3D medical images? (2) How to align image and text features and learn multi-model representations? (3) How to obtain a lightweight language model for our CAD purpose? Inspired by BLIP-2 Li et al. [2023], we propose MedBLIP as shown in Fig. 1, a bootstrapping language-image pre-training model to fuse 3D medical images and texts based on a query mechanism. We first adopt a learnable patch embedding to bridge the gap between 3D medical images and a pre-trained image encoder, which greatly reduces the amount of image data required for learning. Then, we propose a MedQFormer, which contains learnable queries to allow aligning visual features with textural ones desired by a language model. Lastly, we choose BioMedLM Venigalla et al. [2022] as our basic language model and fine-tune it using the LoRA Hu et al. [2021] technique. Our CAD model MedBLIP is lightweight and trainable on a single NVIDIA RTX 3090 GPU.

To train and evaluate the effectiveness of our proposed MedBLIP model, we collect more than 30,000 medical image volumes from five public AD datasets, including ADNI Petersen et al. [2010], NACC Beekly et al. [2007], OASIS Marcus et al. [2007], AIBL Ellis et al. [2009], and MIRIAD Malone et al. [2013]. After pre-training on most of the images from ADNI, NACC, and OASIS datasets, we evaluate our MedBLIP on two tasks: (1) zero-shot classification, which directly applies pre-trained MedBLIP to classify unseen subjects from AIBL and MIRIAD datasets into three classes, i.e., normal controls (NC), mild cognitive impairment (MCI), and AD; and (2) zero-shot medical visual question answering (VQA), which generates an initial diagnosis for an unseen AIBL or MIRIAD subject based on input images and text descriptions and also provides some reasons for making such decision.

Overall, our contributions of this paper are summarized below:

- We propose a lightweight CAD system MedBLIP, which is pre-trained on electronic health records in the form of images and texts, performs zero-shot classification, and makes medical VQA. The architecture of our CAD system is general and has the potential to incorporate more modalities and extend to other diseases beyond AD.
- We propose a MedQFormer module, which extracts 3D medical image features and aligns them with textural features to be fused into a language model (LM). This module provides a way to align different types of medical data into the common space of LM, which is generic and could be used in other medical applications.
- To our best knowledge, we have collected the largest public dataset for studying AD. On this dataset, our MedBLIP achieves the SOTA performance on separating AD and MCI subjects from healthy controls. Besides, we directly work on raw images without any preprocessing, which makes our system easy to use in practice.

2 Related Works

Vision Language Pre-Training. Data collected from different modalities typically provide different views about the data, which often complement each other and provide more complete information

to facilitate a holistic understanding of the data. Vision-language pre-training (VLP) aims to learn multimodal foundation models, showing improved performance on various vision-and-language tasks Radford et al. [2021]. Roughly, we can divide current VLP models into two categories when fusing multi-modal inputs: light fusion and heavy fusion.

The approaches in the light fusion category focus on multi-modal alignment, which facilitates text matching, retrieval, and other downstream tasks, with representative methods like CLIP Radford et al. [2021] and ALIGN Jia et al. [2021]. These methods directly align image representations with the corresponding text representations using a contrastive loss. DeCLIP Li et al. [2021a] exploits inter/intra-modality supervision to train a CLIP-like model with fewer data. On the other hand, the heavy fusion category focuses on incorporating multi-modal information with an attention mechanism to perform additional tasks. For instance, ALBEF Li et al. [2021b] proposes a contrastive alignment, which is followed by deeper fusion with a multi-modal encoder. Methods such as BLIP Li et al. [2022], MoCo He et al. [2020], CoCa Yu et al. [2022] incorporate a decoder and add image-to-text generation as an auxiliary task. Heavy fusion can interpret VQA, captions, and other downstream tasks that require more information for fusion and understanding.

Medical image-text representation learning has been investigated based on contrastive learning as well. CheXzero Tiu et al. [2022] directly applies the CLIP on large-scale chest X-ray datasets to enable zero-shot classification of unseen findings in images. MedCLIP Wang et al. [2022] decouples paired images and texts and uses soft targets of semantic similarities to learn from unpaired medical images and texts. BioViL-T Bannur et al. [2023] proposes a novel multi-image encoder to augment the current image representation with information from previous images. Most existing medical VLP are designed based on 2D images, since compared to 3D image volumes, 2D slices are sufficient to form a large-scale dataset for learning. However, in this paper, we aim to develop a medical VLP based on 3D image volumes with relatively few parameters and limited data size, i.e., a lightweight medical VLP for learning a 3D medical image and text representation.

LLMs for Multi-Modal Understanding. Recently, using large language models (LLMs) as decoders in vision-language tasks has gained significant attention. This approach takes advantage of cross-modal transfer, which allows sharing knowledge between language and multi-modal domains. VisualGPT Chen et al. [2022] and Frozen Tsimpoukelli et al. [2021] have demonstrated the advantage of employing a pre-trained language model as a vision-language model decoder. Flamingo Alayrac et al. [2022] freezes a pre-trained vision encoder and language model and then fuses vision and language modalities with gated cross-attention. BLIP-2 Li et al. [2023] designs a Q-Former to align the visual features from the frozen visual encoder with large language models, like FLAN-T5 Chung et al. [2022] and OPT Zhang et al. [2022]. FROMAGe Koh et al. [2023] freezes large language models and visual encoders, and fine-tunes linear mapping layers to achieve cross-modality interactions. This method shows strong zero-shot performances on contextual image retrieval and multi-modal dialogue tasks. Built upon PaLM Chowdhery et al. [2022], PaLM-E Driess et al. [2023] employs features from sensor modalities and integrates real-world continuous sensor modalities into an LLM, thereby establishing a connection between real-world perceptions and human languages. GPT-4 OpenAI [2023] presents powerful visual understanding and reasoning abilities after pre-training on a vast collection of image-text data.

Most recently, several domain-specific multi-modal LLMs have been developed. ChatCAD Wang et al. [2023] combines visual and linguistic information processed by various networks as inputs of large language models to develop a medical-image CAD model, which provides a condensed report and offers interactive explanations and medical recommendations. Open-ended MedVQA van Sonsbeek et al. [2023] employs a multi-layer perceptron (MLP) network that maps the extracted visual features from a frozen vision encoder to a set of learnable tokens, which develops an open-ended VQA for diagnoses and treatment decisions. Differently, our MedBLIP explores a lightweight framework that works on 3D medical scans and aligns different types of medical data for CAD.

3 MedBLIP

3.1 Problem Formulation

We design a CAD system in the form of dialogue, with application to automatic AD diagnosis. Given inputs of a brain image scan I collected from a subject and a textual description T generated from this subject's EHRs in natural language, for a question asked in natural language Q, our CAD aims to

sequentially generate an answer $A = \{A_0, A_1, ..., A_N\}$ composed of N tokens, by conditioning on all inputs $\{I, T, Q\}$. To achieve this goal, we build a CAD model based on a large language model and find its optimal parameters θ^* by maximizing the conditional log-likelihood below:

$$\theta^* = \arg\max_\theta \sum_{i=1}^N \log p_\theta \left(\mathbf{A}_i \mid \mathbf{I}, \mathbf{T}, \mathbf{Q}, \mathbf{A}_{i-1} \right). \tag{1}$$

3.2 Network Framework

Our CAD model is designed as an encoder-decoder architecture, with a two-stream encoder and a language model (LM) as a decoder, as illustrated in Fig. 1. Specifically, the two-stream encoder takes inputs from two modalities, namely a vision sub-encoder for the image I and the text sub-encoder for the textual description T and the question Q. The language model is defined as a causal language transformer, which generates the answer A in an auto-regressive manner.

Vision Encoding Stream. To encode a brain image volume and fully leverage an existing large model for reducing data requirements, we employ a pre-trained 2D vision encoder to extract its 3D visual features. To make this work, we need to address two problems: (1) bridging the domain and dimension gaps between a 2D vision encoder and a 3D medical scan, and (2) aligning image features with textural ones, which allows mapping all inputs into the latent space of the LM decoder for learning multi-modal representations. Inspired by Li et al. [2023], we propose a query network based on a transformer encoder, which maps the visual features into a visual prefix $H_v = \{v_1, v_2, \cdots, v_{\ell_v}\} \in \mathbb{R}^{\ell_v \times e}$ for the language model, where ℓ_v is the length of the vision embedding sequence and e is the embedding size. Also, we have a lightweight projection, which is learnable and adapts 3D image volumes to inputs of a pre-trained image encoder. This medical query transformer (MedQFormer) tackles the above two problems and will be discussed in detail in Sect. 3.3.

Language Encoding Stream. Regarding the textural description of subjects' EHRs except for image scans and the asked questions, we first utilize a standard tokenization process as in Jain [2022] to obtain a sequence of tokens, i.e., the textual description $\mathbf{T} = \{t_1, t_2, \cdots, t_{\ell_t}\} \in \mathbb{R}^{\ell_t \times e}$, the question $\mathbf{Q} = \{q_1, q_2, \cdots, q_{\ell_q}\} \in \mathbb{R}^{\ell_q \times e}$, and the answer $\mathbf{A} = \{a_1, a_2, \cdots, a_{\ell_a}\} \in \mathbb{R}^{\ell_a \times e}$, where ℓ_t, ℓ_q, ℓ_a indicate the length of the embedding sequence of the text, question, and answer, respectively. These tokens are embedded later using the embedding function provided in a pre-trained language model.

Prompt Structure. To create a structured prompt, following current VQA methods used in language models Li et al. [2023], van Sonsbeek et al. [2023], we prepend the question and answer tokens with tokenized descriptive strings, namely in the form of **question:** and **answer:**. We choose to place the embeddings of the image and text description before the question tokens. As a result, we have the following prompt template:

$$\begin{aligned} p = [&v_1, v_2, \cdots, v_{\ell_x}, t_1, t_2, \cdots, t_{\ell_t}, \textbf{Question } : What \\ &will\ this\ subject\ be\ diagnosed\ with? \textbf{Answer:}], \end{aligned} \tag{2}$$

which is fed as input to the language model below.

Language Model. Following standard language modeling systems Venigalla et al. [2022], we treat VQA as a process of a conditional generation of text, and we optimize the standard maximum likelihood objective during training. The language model receives the prompt sequence as input and outputs the answer A, token by token. Specifically, at each time step i, the outputs of the model are the logits, which parameterize a categorical distribution $p_\theta(A)$ over the vocabulary tokens. This distribution is represented as follows:

$$\log p_\theta(\mathbf{A}) = \sum_{l_a} \log p_\theta \left(a_i \mid v_1, \ldots v_{\ell_v}, t_1, \ldots t_{\ell_t}, q_1, \ldots q_{\ell_q}, a_1, \ldots a_{i-1} \right). \tag{3}$$

The parameters of the language model are initialized from a pre-trained model, which has been previously pre-trained on huge web-collected datasets Dodge et al. [2021], Gao et al. [2020].

3.3 MedQFormer

To bridge the gap between 3D medical images and 2D vision encoders pre-trained on natural images, inspired by BLIP-2 Li et al. [2023], we employ a query encoder to extract and align vision features.
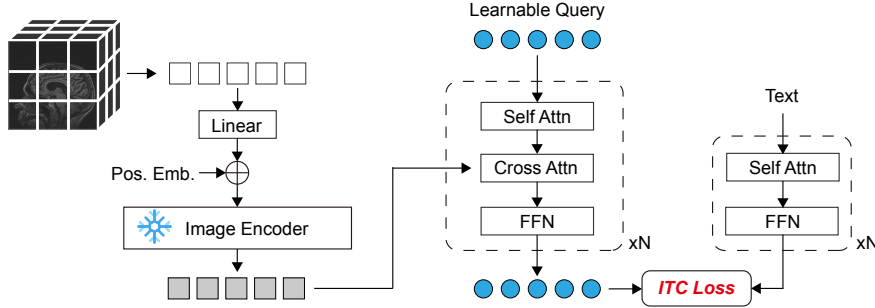
Figure 2: Illustration of our proposed MedQformer that aligns 3D visual and textural features for learning in the unified latent space of language model.

Image Feature Extraction. We first divide the input image I into a set of 3D sub-volumes $\{Iv_i\}_{i=1}^{N_v}$, followed by a linear projection f_{φ_1} that projects 3D cubes into 1D image embeddings $\{E_i = f_{\varphi_1}(Iv_i)\}_{i=1}^{N_v}$. With the addition of learnable position embeddings f_{φ_2}, the image embeddings can be received as inputs of a standard pre-trained vision encoder to extract desired image features. Although the pre-trained vision encoder f_ϕ has fixed parameters ϕ, we have learnable linear projection and position embedding to transfer a 2D vision encoder to a 3D medical domain. Hence, we have a medical vision encoder with learnable parameters φ_1 and φ_2, which maps a volumetric image I into N_v visual features $f_1, \cdots, f_{N_v} = \{f_\phi(f_{\varphi_1}(Iv_i), f_{\varphi_2}(Iv_i))\}_{i=1}^{N_v}$. As a result, we obtain the final image embeddings $IE = (f_i, \cdots, f_{N_v})$ for each input image volume I.

Query Encoder. To map the visual features $\{f_i\}_{i=1}^{N_v}$ into the common language space, we use a set of L learnable queries $qry_i \in \mathbb{R}^{d_e}$, where d_e is the dimension of query embeddings. These queries have a transformer structure that interacts with the image encoder for adjusting visual feature extraction and a text transformer as a textural feature extractor. As shown in Fig. 2, these learnable queries interact with each other through self-attention layers, then interact with image features through cross-attention layers. As a result, we obtain a visual prefix H_v that is aligned with textural features and can be taken by a language model.

3.4 Training MedBLIP

Learnable Parameters. Standard fine-tuning of a language model could hurt its generalization capability, especially if a dataset used for fine-tuning has a small size and is domain-specific as in our case. Therefore, we consider two parameter-efficient strategies that adapt the attention blocks of language models:

- **Frozen LM.** The parameters of the language model are kept entirely frozen during training. In this setting, only the 3D vision query network is updated through backpropagation.
- **Low-Rank Adaptation (LoRA).** We add learnable weight matrices to the query Q_w and value V_w of the attention blocks in each layer of the frozen language model as $W + \triangle W$ following Hu et al. [2021]. In this setting, the 3D vision query network function is trained together with the learnable weight matrices.

Objective Functions. We have loss functions for MedQformer and LM modules in our MedBLIP model. As discussed in Sect. 3.3, MedQformer includes both a transformer image encoder E_I and a transformer text encoder E_T. During training, we have a set of image-text pairs (I, T) and a set of image and diagnosis Q&A pairs (I, Q&A). We use the image-text contrastive learning (ITC) loss in Radford et al. [2021] to align multi-modal representation, resulting in our feature alignment loss:

$$\mathcal{L}_{FA} = contrastive\left(E_I(I), E_T(T)\right) + contrastive\left(E_I(I), E_T(Q\&A)\right). \quad (4)$$

Similar to BLIP-2 Li et al. [2023], we select the one that has the highest similarity with text from multiple output query embeddings to compute the ITC Loss. To supervise the LM component, we use cross entropy to compute language generation loss $\mathcal{L}_{LG}$. Hence, the final loss function is defined as:

$$\mathcal{L}_{total} = \mathcal{L}_{FA} + \lambda_{LG}\mathcal{L}_{LG}, \quad (5)$$

where λ_{LG} is a hyperparameter to balance these two terms.

Table 1: Demographic statistics of used AD datasets. F: female, M: male, Educ: Education level, SES: Socio-Economic Status, MMSE: Mini-Mental State Examination, CDR: Clinical Dementia Rate, E/L/S/PMCI: early, late, stable, and progressive MCI, IMCI: Impaired not MCI, and DEM: demented. # indicates the number.

Datasets	#Images	Texts							
		#F/#M	Age(#)	Educ(#)	SES(#)	MMSE(#)	CDR(#)	Logical Memory(#)	Diagnosis(#)
ADNI	10387	4710/5677	45-95(10386)	9860	-	9385	9401	7189	NC,MCI,E/L/S/PMCI,AD (10387)
NACC	15354	9058/6296	19-102(15354)	15329	-	7867	15354	7654	NC, IMCI, MCI, DEM (14277)
OASIS	3020	1798/1222	18-98(3020)	2300	2153	2293	2300	-	DEM, Non-DEM (336)
AIBL	1002	471/531	42-96(1002)	-	-	1002	1002	1002	NC, MCI, AD (997)
MIRIAD	708	393/315	55-87(708)	-	-	268	46	-	NC, AD(708)

4 Experiments

4.1 Datasets and Experimental Settings

We collect more than 30,000 image volumes from five public datasets for studying AD/Dementia and evaluate our CAD system MedBLIP on separating subjects with AD or mild cognitive impairment (MCI) from normal controls (NC). Table 1 reports the demographic statistics of these five datasets.

ADNI Petersen et al. [2010]. This dataset has 10,387 volumetric T1 MRI scans that went through a series of pre-processing steps, including denoising, bias field correction, skull stripping, and affine registration to the SRI24 atlas, with an image size of $138 \times 176 \times 138$. For testing, we subject-wisely sample a subset of 200 images in each class (i.e., NC, MCI, AD), which is named ADNI-3x200.

NACC Beekly et al. [2007]. This dataset has a large amount of raw volumetric T1 MRI scans with a variety of resolutions. We select those MRIs having $100\sim256$ slices in all three dimensions, resulting in 15,354 images. Unlike the ADNI dataset, we directly use the raw data; but similarly, we sample subject-wisely a NACC-3x200 dataset for testing.

OASIS Marcus et al. [2007]. We collect 3020 volumetric T1 MRIs from OASIS 1&2. These scans went through pre-processing with denoising and skull stripping and have a size of $256 \times 256 \times 256$. Since OASIS 1 only releases some clinical reports but with no diagnoses (e.g. NC, MCI or dementia), we use all images from OASIS 1 for pre-training. For testing, we sample subject-wisely an OASIS-2x200 subset from OASIS 2 to separate demented and non-demented subjects.

AIBL Ellis et al. [2009]. This dataset has 1002 volumetric T1 MRI scans with sizes of $160 \times 240 \times 256$, which are collected from demented, MCI, or healthy subjects. We do not use this data for training; for testing, we sample a balanced subset with 200 images each for NC, MCI, and dementia classes.

MIRIAD Malone et al. [2013]. We collect 708 raw volumetric T1 MRI scans, which have an image size of $124 \times 256 \times 256$. This is a binary classification dataset with two labels, i.e., demented and not-demented subjects. We sample a balanced subset with a 1:1 positive and negative ratio, resulting in 2×200 images for testing. No images are used for training to perform zero-shot experiments.

As a result, we have most images from ADNI, NACC, and OASIS datasets for pretraining and save images from AIBL and MIRIAD datasets for zero-shot testing. In total, we held 1000 subjects with 2600 samples out for evaluation. To simplify the preprocessing step, all images are first padded to a cube and then scaled to a unified size of $224 \times 224 \times 224$ as inputs.

Implementation Details. For the frozen image encoder, we choose state-of-the-art pre-trained ViT-G/14 from EVA-CLIP Fang et al. [2022], which is demonstrated to be effective in BLIP-2 Li et al. [2023]. For the input image with a size of $224 \times 224 \times 224$, the patch size and the stride are both set as 32, resulting in image features with the size of 344×1408. For the MedQformer, we use 32 learnable queries, where each query has a dimension of 768 and the hidden layers N is set to 12. Regarding language models, we have three options, i.e., FLAN-T5 Chung et al. [2022], BioGPT Luo et al. [2022], and BioMedLM Venigalla et al. [2022]. FLAN-T5 is an instruction-trained model with 3B parameters trained on C4 WebText Dodge et al. [2021]. BioGPT and BioMedLM are both GPT models relying on GPT-2 architecture, pre-trained on PubMed and biomedical data from the Pile Gao et al. [2020], with a size of 1.5B and 2.7B parameters, respectively. All our models are able to fine-tune on a single NVIDIA RTX 3090 GPU. We use the AdamW optimizer with a learning rate of 5e-3. The hyperparameter λ_{LG} is set to 1.

Table 2: Experimental results of our MedBLIP on five datasets, including zero-shot CAD on the last two datasets. The classification performance is measured in the mean accuracy (ACC) with five runs. The best scores are in bold.

Methods		LM size	#Learnable params	ADNI -3x200	NACC -3x200	OASIS -2x200	AIBL	MIRIAD
FLAN-T5 Chung et al. [2022]	Text only		-	37.0%	39.5%	46.7%	33.3%	60.0%
Ours w/ T5	Frozen	3.4B	151M	50.5%	69.2%	61.3%	54.7%	64.0%
	LoRA		156M	64.0%	77.3%	75.8%	59.2%	66.8%
BioGPT Luo et al. [2022]	Text only		-	25.7%	21.7%	28.3%	26.7%	50.0%
Ours w/ BioGPT	Frozen	1.5B	151M	56.3%	66.5%	66.0%	60.7%	55.2%
	LoRA		156M	62.2%	72.3%	71.7%	62.4%	59.7%
BioMedLM Venigalla et al. [2022]	Text only		-	62.5%	63.5%	61.8%	65.7%	46.3%
Ours w/ BioMedLM	Frozen	2.7B	151M	71.2%	82.0%	79.8%	77.8%	66.1%
	LoRA		154M	**78.7%**	**83.3%**	**85.3%**	**80.8%**	**71.0%**

I: T: 78-year-old Male. The MMSE score is 21. The CDR is 0.5. The logical memory score is 2.

Q: What will this subject be diagnosed with?

Ground Truth A: Dementia.

Our A: Dementia.   a

I: T: 85-year-old Female. The MMSE score is 30. The CDR is 0.

Q: What will this subject be diagnosed with?

Ground Truth A: Mild cognitive impairment.

Our A: Mild cognitive impairment.   b

I: T: 78-year-old Female. The MMSE score is 27. The CDR is 0.5. The logical memory score is 5.

Q: What will this subject be diagnosed with?

Ground Truth A: Healthy.

Our A: Healthy.   c

I: T: 82.2-year-old Female, with 16 years of education. The MMSE score is 27. The CDR score is 0.5.

Q: What will this subject be diagnosed with?

Ground Truth A: Mild cognitive impairment.

Our A: Mild cognitive impairment.

Q: Why have you made this decision?

Our A: CDR score is 0.5.   d

I: T: 63-year-old Female. The MMSE score is 18. The CDR is 1. The logical memory score is 5.

Q: What will this subject be diagnosed with?

Ground Truth A: Dementia.

Our A: Dementia.

Q: What is abnormal in the brain imaging?

Our A: The brain is atrophic.   e

I: T: 71.6-year-old Male, with 16 years of education. The MMSE score is 30. The CDR score is 0. The logical memory score is 14.

Q: What will this subject be diagnosed with?

Ground Truth A: Healthy.

Our A: Healthy.

Q: What is the reason for you decision?

Our A: The MMSE socre is higher than the CDR score and the logical memory score is higher than the Dementia score.   f
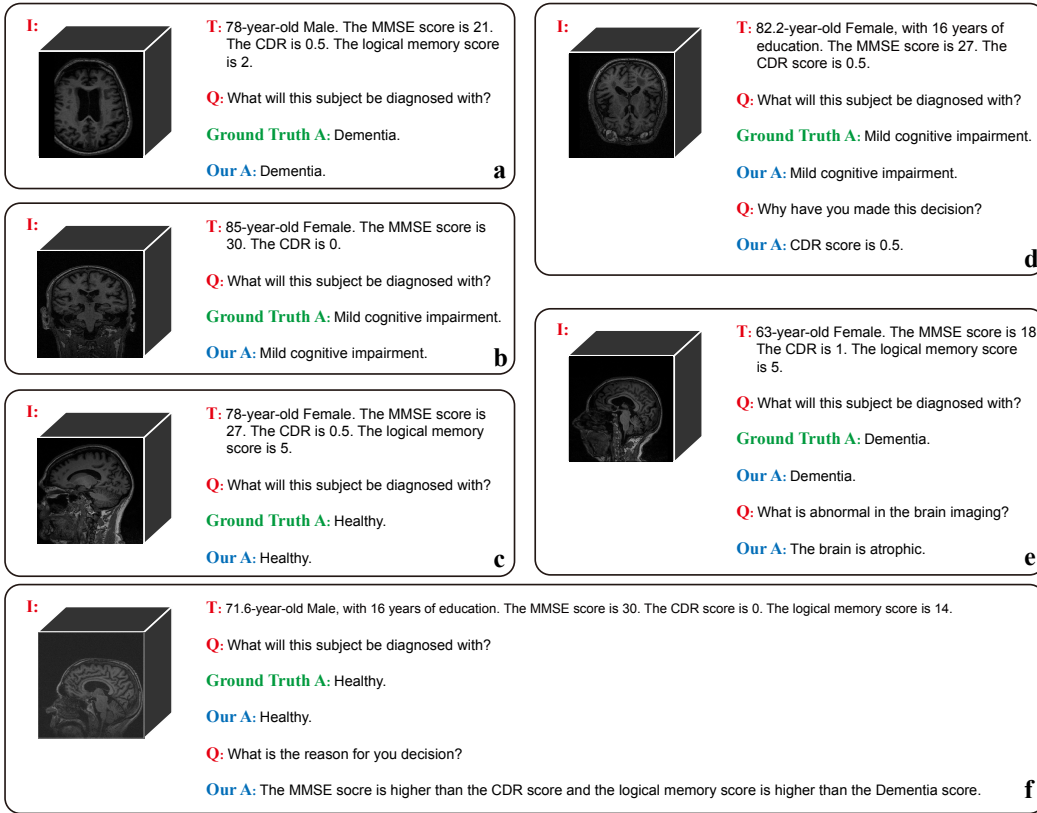
Figure 3: Samples of zero-shot results on the AIBL dataset, which are generated by our MedBLIP built on BioMedLM with LoRA fine-tuning.

4.2 Experimental Results

Zero-shot Medical CAD. Table 2 reports the evaluation of our MedBLIP using different language models and settings. The language models, i.e., FLAN-T5, BioGPT, and BioMedLM, show their capability of performing monomodal medical CAD, i.e., using text descriptions only, to some extent. Among these three language models, BioMedLM performs the best, showing that it captures some dependencies between prompts and inherent knowledge when generating answers. By adding the visual modality even without fine-tuning, the performance of our model on all datasets has improved significantly. The accuracy improvement varies within [4.0%, 44.8%], and the BioGPT benefits the most from the visual input. This result indicates the necessity of using image scans in diagnosis. Using the fine-tuning technique LoRA, our performance is further improved, with at least 1.3% and

Table 3: Comparison between a large vision encoder and our MedQFormer on ADNI.

Visual features	#Params	Accuracy
ViT-G Fang et al. [2022]	1B	72.2%
Our MedQFormer	151M	71.6%

Table 4: Comparison between different prompt structures.

Setting	ADNI -3x200	NACC -3x200	OASIS -2x200	AIBL	MIRIAD
Regular (I&T, Q, A)	78.7%	83.3%	85.3%	80.8%	71.0%
Alternative (Q, I&T, A)	79.3%(+0.6)	82.8%(-0.5)	82.5%(-1.8)	82.8%(+2.0)	70.8%(+0.2)

at most 14.5% improvement in accuracy. Overall, our MedBLIP built upon BioMedLM and LoRA fine-tuning shows the best performance on all datasets.

Figure 3 (a-c) visualizes the zero-shot CAD process on unseen subjects sampled from the AIBL dataset. Take Fig. 3(b) for example, although the text description of this subject shows no significant difference from those of healthy subjects, in brain scans the hippocampus and ventricle show the presence of abnormal atrophy. Our MedBLIP provides the correct diagnosis of MCI.

Zero-shot Medical VQA. Figure 3 (d-f) shows the zero-shot Medical Visual question answering(VQA) ability of our MedBLIP. Since our approach is generative, after a simple classification-based question, MedBLIP provides a natural way of performing VAQ and presents the chain of thoughts. MedBLIP may also generate unsatisfactory answers to users' questions due to various reasons, including inaccurate medical knowledge from the LLM, activating the incorrect reasoning path, or not having up-to-date information about new image content.

Ablation Study. We perform ablation studies from three aspects to answer the following three questions: (1) Why use a 2D pre-trained vision encoder instead of a trainable large vision encoder? (2) Will a prompt structure make a difference in the final CAD result? and (3) Why need the ITC loss between the image and diagnosis Q&A?

(1) Benefit of using a frozen 2D pre-trained vision encoder. To demonstrate the effectiveness of our lightweight image encoder based on the 2D pre-trained model, we take the query output embedding from MedQformer and compare it with features extracted from trainable ViT-G Fang et al. [2022] on ADNI. We add a linear classification head with the cross-entropy loss. Table 3 reports that MedQFormer achieves slightly reduced performances, i.e., 0.6% lower than ViT-G in accuracy, but with much fewer parameters (only 15.1% of ViT-G's). This lightweight module benefits downstream tasks and allows building our model on language models and training it on one GPU. We can also see that benefiting from this lightweight visual encoder, our MedBLIP outputs ViT-G by an improvement of 6.5% in the classification accuracy on ADNI.

(2) Effect of using different prompt structures. To answer the second question above, we investigate the order of three prompting components, i.e., image and text features, the question, and the answer, and its effect on our model's performance. We treat the one with the question in the middle as the regular prompt structure and compare it to the one starting with the question. Table 4 shows that on some datasets our MedBLIP prefers the regular prompt, but this is not always the case. We conclude that the prompt strategy will not make a huge difference in the final performance of our model.

(3) Necessity of using two ITC loss functions. Besides the regular ITC loss between image and text pairs, we have another one between image and diagnosis Q&A, as presented in Eq. 4. Table 5 demonstrates that by adding the second ITC loss function, the classification accuracy improves on

Table 5: Ablation study on loss functions.

Loss Function	ADNI -3x200	NACC -3x200	OASIS -2x200	AIBL	MIRIAD
$contrastive(I, T)$	71.7%	80.5%	82.5%	74.7%	66.8%
$contrastive(I, T) + contrastive(I, Q\&A)$	78.7%(+7.0)	83.3%(+2.8)	85.3%(+2.8)	80.8%(+6.1)	71.0%(+4.2)

all datasets. This result is consistent with our motivation of adding the ITC loss between image and diagnosis Q&A, since it enforces the learnable queries to extract image features related to CAD.

5 Discussion and Conclusion

In this paper, we propose a novel CAD system MedBLIP that fuses medical multi-modal data, i.e., image and text, from EHRs and shows its capability of performing zero-shot classification and medical VQA. Our MedBLIP introduces MedQFormer, a lightweight trainable 3D vision encoder that acts as a bridge between 3D medical images and a large frozen 2D vision encoder and as a bridge between 3D medical images and language models. Moreover, MedBLIP operates with low computational costs, as it smartly combines large pre-trained vision and language models with no need of training them from scratch or a large dataset in a specific medical domain. Our experiments demonstrate the effectiveness of our approach by outperforming several baselines, which sheds new light on further exploring medical multi-modal CAD.

Limitations and Future Work. LLMs can perform in-context learning given domain-specific few-shot examples. However, in our experiments with MedBLIP, we do not observe an improved VQA performance when asking something about the input brain scan context, even though it made the correct diagnosis. We attribute the unsatisfactory VQA results to the lack of corresponding textural descriptions of brain scans in our dataset. Without a description of a 3D brain MRI scan, the LLMs have difficulty describing what they "observe" in this image, such as the shrunken hippocampus or the enlarged ventricles. Currently, no such dataset or model is available to provide an image caption/description for a brain scan. We will explore this direction in our future work.

Besides, degenerative diseases like AD are often studied in the longitudinal setting since longitudinal atrophy has probably happened at an early stage of AD, making it easier to separate MCI subjects from normal controls. In future work, we will extend our model to take longitudinal inputs and further improve our classification accuracy. In addition, in our experiments, we only consider two modalities, i.e., MRIs and texts, other medical data sources, like positron emission tomography (PET) images, and audio, are also useful in diagnosing AD. Fortunately, the architecture of our MedBLIP is flexible enough to incorporate additional modalities, which is also left as our future work.

References

Ronald Carl Petersen, Paul S Aisen, Laurel A Beckett, Michael C Donohue, Anthony Collins Gamst, Danielle J Harvey, Clifford R Jack, William J Jagust, Leslie M Shaw, Arthur W Toga, et al. Alzheimer's disease neuroimaging initiative (adni): clinical characterization. *Neurology*, 74(3): 201–209, 2010.

Duane L Beekly, Erin M Ramos, William W Lee, Woodrow D Deitrich, Mary E Jacka, Joylee Wu, Janene L Hubbard, Thomas D Koepsell, John C Morris, Walter A Kukull, et al. The national alzheimer's coordinating center (nacc) database: the uniform data set. *Alzheimer Disease & Associated Disorders*, 21(3):249–258, 2007.

Daniel S Marcus, Tracy H Wang, Jamie Parker, John G Csernansky, John C Morris, and Randy L Buckner. Open access series of imaging studies (oasis): cross-sectional mri data in young, middle aged, nondemented, and demented older adults. *Journal of cognitive neuroscience*, 19(9):1498–1507, 2007.

Alec Radford, Jong Wook Kim, Chris Hallacy, Aditya Ramesh, Gabriel Goh, Sandhini Agarwal, Girish Sastry, Amanda Askell, Pamela Mishkin, Jack Clark, et al. Learning transferable visual models from natural language supervision. In *International conference on machine learning*, pages 8748–8763. PMLR, 2021.

Junnan Li, Dongxu Li, Caiming Xiong, and Steven Hoi. Blip: Bootstrapping language-image pre-training for unified vision-language understanding and generation. In *International Conference on Machine Learning*, pages 12888–12900. PMLR, 2022.

Junnan Li, Dongxu Li, Silvio Savarese, and Steven Hoi. Blip-2: Bootstrapping language-image pre-training with frozen image encoders and large language models. *arXiv preprint arXiv:2301.12597*, 2023.

Hangbo Bao, Wenhui Wang, Li Dong, Qiang Liu, Owais Khan Mohammed, Kriti Aggarwal, Subhojit Som, Songhao Piao, and Furu Wei. Vlmo: Unified vision-language pre-training with mixture-of-modality-experts. *Advances in Neural Information Processing Systems*, 35:32897–32912, 2022.

Mengde Xu, Zheng Zhang, Fangyun Wei, Yutong Lin, Yue Cao, Han Hu, and Xiang Bai. A simple baseline for zero-shot semantic segmentation with pre-trained vision-language model. *arXiv preprint arXiv:2112.14757*, 2021.

Zifeng Wang, Zhenbang Wu, Dinesh Agarwal, and Jimeng Sun. Medclip: Contrastive learning from unpaired medical images and text. *arXiv preprint arXiv:2210.10163*, 2022.

A Venigalla, J Frankle, and M Carbin. Biomedlm: a domain-specific large language model for biomedical text. *MosaicML. Accessed: Dec*, 23, 2022.

Edward J Hu, Yelong Shen, Phillip Wallis, Zeyuan Allen-Zhu, Yuanzhi Li, Shean Wang, Lu Wang, and Weizhu Chen. Lora: Low-rank adaptation of large language models. *arXiv preprint arXiv:2106.09685*, 2021.

Kathryn A Ellis, Ashley I Bush, David Darby, Daniela De Fazio, Jonathan Foster, Peter Hudson, Nicola T Lautenschlager, Nat Lenzo, Ralph N Martins, Paul Maruff, et al. The australian imaging, biomarkers and lifestyle (aibl) study of aging: methodology and baseline characteristics of 1112 individuals recruited for a longitudinal study of alzheimer's disease. *International psychogeriatrics*, 21(4):672–687, 2009.

Ian B Malone, David Cash, Gerard R Ridgway, David G MacManus, Sebastien Ourselin, Nick C Fox, and Jonathan M Schott. Miriad—public release of a multiple time point alzheimer's mr imaging dataset. *NeuroImage*, 70:33–36, 2013.

Chao Jia, Yinfei Yang, Ye Xia, Yi-Ting Chen, Zarana Parekh, Hieu Pham, Quoc Le, Yun-Hsuan Sung, Zhen Li, and Tom Duerig. Scaling up visual and vision-language representation learning with noisy text supervision. In *International Conference on Machine Learning*, pages 4904–4916. PMLR, 2021.

Yangguang Li, Feng Liang, Lichen Zhao, Yufeng Cui, Wanli Ouyang, Jing Shao, Fengwei Yu, and Junjie Yan. Supervision exists everywhere: A data efficient contrastive language-image pre-training paradigm. *arXiv preprint arXiv:2110.05208*, 2021a.

Junnan Li, Ramprasaath Selvaraju, Akhilesh Gotmare, Shafiq Joty, Caiming Xiong, and Steven Chu Hong Hoi. Align before fuse: Vision and language representation learning with momentum distillation. *Advances in neural information processing systems*, 34:9694–9705, 2021b.

Kaiming He, Haoqi Fan, Yuxin Wu, Saining Xie, and Ross Girshick. Momentum contrast for unsupervised visual representation learning. In *Proceedings of the IEEE/CVF conference on computer vision and pattern recognition*, pages 9729–9738, 2020.

Jiahui Yu, Zirui Wang, Vijay Vasudevan, Legg Yeung, Mojtaba Seyedhosseini, and Yonghui Wu. Coca: Contrastive captioners are image-text foundation models. *arXiv preprint arXiv:2205.01917*, 2022.

Ekin Tiu, Ellie Talius, Pujan Patel, Curtis P Langlotz, Andrew Y Ng, and Pranav Rajpurkar. Expert-level detection of pathologies from unannotated chest x-ray images via self-supervised learning. *Nature Biomedical Engineering*, pages 1–8, 2022.

Shruthi Bannur, Stephanie Hyland, Qianchu Liu, Fernando Perez-Garcia, Maximilian Ilse, Daniel C Castro, Benedikt Boecking, Harshita Sharma, Kenza Bouzid, Anja Thieme, et al. Learning to exploit temporal structure for biomedical vision-language processing. *arXiv preprint arXiv:2301.04558*, 2023.

Jun Chen, Han Guo, Kai Yi, Boyang Li, and Mohamed Elhoseiny. Visualgpt: Data-efficient adaptation of pretrained language models for image captioning. In *Proceedings of the IEEE/CVF Conference on Computer Vision and Pattern Recognition*, pages 18030–18040, 2022.

Maria Tsimpoukelli, Jacob L Menick, Serkan Cabi, SM Eslami, Oriol Vinyals, and Felix Hill. Multimodal few-shot learning with frozen language models. *Advances in Neural Information Processing Systems*, 34:200–212, 2021.

Jean-Baptiste Alayrac, Jeff Donahue, Pauline Luc, Antoine Miech, Iain Barr, Yana Hasson, Karel Lenc, Arthur Mensch, Katherine Millican, Malcolm Reynolds, et al. Flamingo: a visual language model for few-shot learning. *Advances in Neural Information Processing Systems*, 35:23716–23736, 2022.

Hyung Won Chung, Le Hou, Shayne Longpre, Barret Zoph, Yi Tay, William Fedus, Eric Li, Xuezhi Wang, Mostafa Dehghani, Siddhartha Brahma, et al. Scaling instruction-finetuned language models. *arXiv preprint arXiv:2210.11416*, 2022.

Susan Zhang, Stephen Roller, Naman Goyal, Mikel Artetxe, Moya Chen, Shuohui Chen, Christopher Dewan, Mona Diab, Xian Li, Xi Victoria Lin, et al. Opt: Open pre-trained transformer language models. *arXiv preprint arXiv:2205.01068*, 2022.

Jing Yu Koh, Ruslan Salakhutdinov, and Daniel Fried. Grounding language models to images for multimodal generation. *arXiv preprint arXiv:2301.13823*, 2023.

Aakanksha Chowdhery, Sharan Narang, Jacob Devlin, Maarten Bosma, Gaurav Mishra, Adam Roberts, Paul Barham, Hyung Won Chung, Charles Sutton, Sebastian Gehrmann, et al. Palm: Scaling language modeling with pathways. *arXiv preprint arXiv:2204.02311*, 2022.

Danny Driess, Fei Xia, Mehdi SM Sajjadi, Corey Lynch, Aakanksha Chowdhery, Brian Ichter, Ayzaan Wahid, Jonathan Tompson, Quan Vuong, Tianhe Yu, et al. Palm-e: An embodied multimodal language model. *arXiv preprint arXiv:2303.03378*, 2023.

OpenAI. Gpt-4 technical report, 2023.

Sheng Wang, Zihao Zhao, Xi Ouyang, Qian Wang, and Dinggang Shen. Chatcad: Interactive computer-aided diagnosis on medical image using large language models. *arXiv preprint arXiv:2302.07257*, 2023.

Tom van Sonsbeek, Mohammad Mahdi Derakhshani, Ivona Najdenkoska, Cees GM Snoek, and Marcel Worring. Open-ended medical visual question answering through prefix tuning of language models. *arXiv preprint arXiv:2303.05977*, 2023.

Shashank Mohan Jain. Hugging face. In *Introduction to Transformers for NLP: With the Hugging Face Library and Models to Solve Problems*, pages 51–67. Springer, 2022.

Jesse Dodge, Maarten Sap, Ana Marasovic, William Agnew, Gabriel Ilharco, Dirk Groeneveld, and Matt Gardner. Documenting the english colossal clean crawled corpus. *arXiv preprint arXiv:2104.08758*, 2021.

Leo Gao, Stella Biderman, Sid Black, Laurence Golding, Travis Hoppe, Charles Foster, Jason Phang, Horace He, Anish Thite, Noa Nabeshima, et al. The pile: An 800gb dataset of diverse text for language modeling. *arXiv preprint arXiv:2101.00027*, 2020.

Yuxin Fang, Wen Wang, Binhui Xie, Quan Sun, Ledell Wu, Xinggang Wang, Tiejun Huang, Xinlong Wang, and Yue Cao. Eva: Exploring the limits of masked visual representation learning at scale. *arXiv preprint arXiv:2211.07636*, 2022.

Renqian Luo, Liai Sun, Yingce Xia, Tao Qin, Sheng Zhang, Hoifung Poon, and Tie-Yan Liu. Biogpt: generative pre-trained transformer for biomedical text generation and mining. *Briefings in Bioinformatics*, 23(6), 2022.